CHINESE OPTICS LETTERS

Vol. 21, No. 6 | June 2023

Sideband-free dispersion-managed Yb-doped mode-locked fiber laser with Gires–Tournois interferometer mirrors

Aoran Feng (丰傲然)[1], Bowen Liu (刘博文)[1,2*], Dongyu Yan (闫东钰)[3**], Genyu Bi (毕根毓)[1,2], Youjian Song (宋有建)[1], and Minglie Hu (胡明列)[1,2]

[1] Ultrafast Laser Laboratory, Key Laboratory of Opto-electronic Information Technology (Ministry of Education), School of Precision Instruments and Opto-electronics Engineering, Tianjin University, Tianjin 300072, China

[2] Georgia Tech Shenzhen Institute, Tianjin University, Shenzhen 518055, China

[3] Optoelectronic Detection and Processing Laboratory, School of Electronic Engineering, Tianjin University of Technology and Education, Tianjin 300222, China

*Corresponding author: bwliu@tju.edu.cn

**Corresponding author: yandongyu@tju.edu.cn

Received February 2, 2023 | Accepted March 24, 2023 | Posted Online June 6, 2023

High-order dispersion introduced by Gires–Tournois interferometer mirrors usually causes spectral sidebands in the near-zero dispersion region of mode-locked fiber lasers. Here, we demonstrate a sideband-free Yb-doped mode-locked fiber laser with dispersion-compensating Gires–Tournois interferometer mirrors. Both the simulation and the experiment demonstrate that the wavelength and energy of the sidebands can be tuned by changing the transmission coefficient of the output mirror, the pump power, and the ratio of the net cavity dispersion to the net third-order dispersion in the cavity. By optimizing these three parameters, the laser can generate a sideband-free, Gaussian-shaped spectrum with a 13.56-nm bandwidth at $-0.0232\ \mathrm{ps}^2$ net cavity dispersion, which corresponds to a 153-fs pulse duration.

Keywords: fiber laser; dispersion compensation; sideband suppression.
DOI: 10.3788/COL202321.061401

1. Introduction

Due to their high peak power and narrow pulse, mode-locked Yb-doped fiber lasers have great potential in scientific and industrial applications, such as laser micromachining, optical imaging, and optical frequency combs[1–7]. In return, the development of other fields has also greatly promoted ultrafast photonics, such as the methods for manipulating ultrafast dynamics[8] and some nanomaterials[9,10], which can be used in the ultrafast lasers to achieve mode-locking. In mode-locked fiber lasers, major pulse-shaping mechanisms include solitons[11], dispersion-managed solitons[12], similaritons, and dissipative solitons[13,14]. Among these mechanisms, the output pulses from dispersion-managed mode-locked fiber lasers feature a wide spectrum, a narrow pulse duration, and a high pulse energy. In order to manage dispersion, we usually introduce some dispersion-compensation components into Yb-doped mode-locked fiber lasers, such as grating pairs, prism pairs, and chirped fiber Bragg gratings.

However, grating pairs introduce positive third-order dispersion and large insertion losses[15]. Prism pairs provide relatively insufficient group delay dispersion (GDD) and occupy a large space[16]. Chirped fiber Bragg gratings are conducive to all-fiber configurations, but they require additional temperature control devices because of their temperature sensitivity[17]. In addition, their reflection bandwidth is much narrower than the gain bandwidth of Yb-doped fibers, which leads to a filtering effect and causes mode-locking instability in the near-zero dispersion region[18]. By contrast, Gires–Tournois interferometer (GTI) mirrors offer attractive advantages, including compactness, high stability, and low insertion loss, and the dispersion that they provide is tunable by changing the reflection times.

In the past three decades, GTI mirrors have been exploited in managing dispersion in mode-locked lasers[19–24]. In 2010, Ren *et al.* designed GTI mirrors for dispersion management in a nonlinear polarization evolution mode-locked fiber laser. The mirrors provided a GDD of $-1000\ \mathrm{fs}^2$ at a center wavelength of 1032 nm. But the net cavity dispersion (NCD) was still positive due to the long fiber length. Consequently, an M-type self-similar soliton mode-locked spectrum was obtained[21]. Currently, there are still researchers using GTI mirrors for

compensating dispersion in Yb-doped fiber lasers and output short pulses[22,23]. For example, in 2021, Jia *et al.* used GTI mirrors with a large amount of GDD in a Yb-doped semiconductor saturable absorber mirror (SESAM) mode-locked fiber laser to compensate for intracavity dispersion. Stable mode locking was achieved over a fairly large range of NCD values. Nevertheless, strong spectral sidebands appeared on the right side of the spectrum when the NCD was close to zero[22]. This phenomenon is also shown in the literature[19,20]. Highly dispersive GTIs always show steep GDD curves, corresponding to a larger high-order dispersion (HOD). The main effect of HOD on solitons is to generate dispersive waves that are superimposed onto the soliton, which results in spectral sidebands when the exact phase-matching condition is met[24,25].

The spectral sidebands not only preempt the soliton energy and limit the spectral width but also lead to interactions between solitons, thereby causing pulse timing jitter and increasing the bit-error-rate over long distances[26,27]. Also, the strong spectral sidebands will take partial energy from main spectral peaks after amplification, which imposes a limit on amplification efficiency[28]. Recently, studies on sidebands and its suppression in Er-doped and Tm-doped nonlinear polarization evolution mode-locked fiber lasers with the method of polarization control and nonlinear Fourier transform were reported[29–32]. However, studies on the sidebands caused by HOD of GTI mirrors and the method of eliminating them in Yb-doped fiber lasers with GTI mirrors have not yet been studied. Simply decreasing the HOD of GTI mirrors will make designing the GTI mirrors and the laser resonator challenging. Therefore, it is essential to explore a way to eliminate sidebands caused by the HOD of the GTI mirrors without complicating the laser resonator, which has strong potential for improving the laser stability and supplying high-quality laser pulses for downstream amplification.

In this work, we propose a comprehensive scheme for mode-locked fiber lasers with GTI mirrors to suppress spectral sidebands in the near-zero dispersion region. Both the numerical and the experimental results demonstrate that the wavelength and energy of the sidebands can be tuned by changing the transmission coefficient of the output mirror, the ratio of the NCD to the NTOD in the cavity, and the pump power. By optimizing these three parameters, a Gaussian-shaped spectrum without sidebands is achieved in the near-zero dispersion region of these lasers.

2. Numerical Simulation and Results

The numerical simulation is shown in Fig. 1. The linear cavity consists of a single-mode polarization-maintaining fiber; a saturable absorber; a Yb-doped polarization-maintaining fiber; two types of GTI mirrors (GTIM1 and GTIM2) with GDDs of $-3000\,\mathrm{fs}^2$ and $-1000\,\mathrm{fs}^2$, respectively; and an output coupling mirror.

In the simulation, the pulse evolution in the fiber laser is modeled by solving the nonlinear Schördinger equation

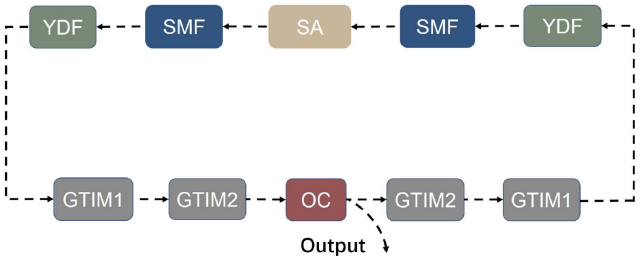

Fig. 1. Numerical simulation model. Saturable absorber, SA; single-mode fiber, SMF; Yb-doped fiber, YDF; optical coupler, OC; GTIM1, GTI mirrors, which provide a GDD of $-3000\ \mathrm{fs}^2$ per reflection; and GTIM2, GTI mirrors, which provide a GDD of $-1000\ \mathrm{fs}^2$ per reflection.

$$\frac{\partial A}{\partial z} - i\sum_{m=2}^{\infty}\frac{\beta_m}{m!}(i\partial_T)^m A - \frac{g}{2\Omega_g^2}\cdot\frac{\partial^2 A}{\partial^2 T^2} = \frac{g}{2}A + i\gamma|A|^2 A, \quad (1)$$

where A is the field envelope, z is the propagation coordinate, and T is the time-delay parameter. In order to explore the influence of fiber dispersion, the HOD is taken into consideration. Then, since the dispersion curve of the fiber is relatively flat, we will neglect the HOD terms beyond m and equal to 4. In Eqs. (1), β_2 is the measured value, and β_3, β_4 are obtained by taking the 1st and 2nd derivative, respectively, of β_2 with respect to ω. In the equation, Ω_g is the gain bandwidth, and γ is the nonlinear parameter. The gain coefficient g is given by

$$g = \frac{g_0}{1 + E/E_{\mathrm{sat}}}, \quad (2)$$

where g_0 is the small-signal gain, E is the pulse energy, and E_{sat} is the gain saturation energy. The parameters and model of the SESAM in the simulation align with the literature[18]. The simulation parameters are consistent with those in the experiment. The Yb-doped gain fiber is 0.28 m, the center wavelength of the gain curve is set at 1030 nm, and the single-mode fiber is 0.32 m. Hence, the total fiber length is 0.6 m. Using the numerical model above, we simulate the mode-locked fiber laser with dispersion-compensating GTI mirrors. If the relative energy change in two consecutive cycles is smaller than 10^{-8}, then we consider that the model has converted to a solution. Mode locking is considered unstable if it does not converge after 2000 cycles. Usually, GTI mirrors with a large GDD have a rapidly increasing GDD curve, as shown in the inset of Fig. 2(a), which will introduce large amounts of HOD into the cavity. As displayed in Fig. 2(a), the NCD curves become relatively steep when using GTI mirrors to compensate dispersion, compared with not using them. In addition, even if we let GTIM1 and GTIM2 provide the same GDD at the center wavelength ($\mathrm{NCD} = -0.0072\,\mathrm{ps}^2$ at 1030 nm after compensating), the NCD curve with GTIM1 reflecting 6 times is steeper than the curve with GTIM2 reflecting 18 times, which means larger HODs are introduced. Then, we compare the simulation spectra between using GTIM1 to reflect 6 times and using GTIM2 to reflect 18 times, as displayed in Fig. 2(b). In order to explore the influence of HOD on our

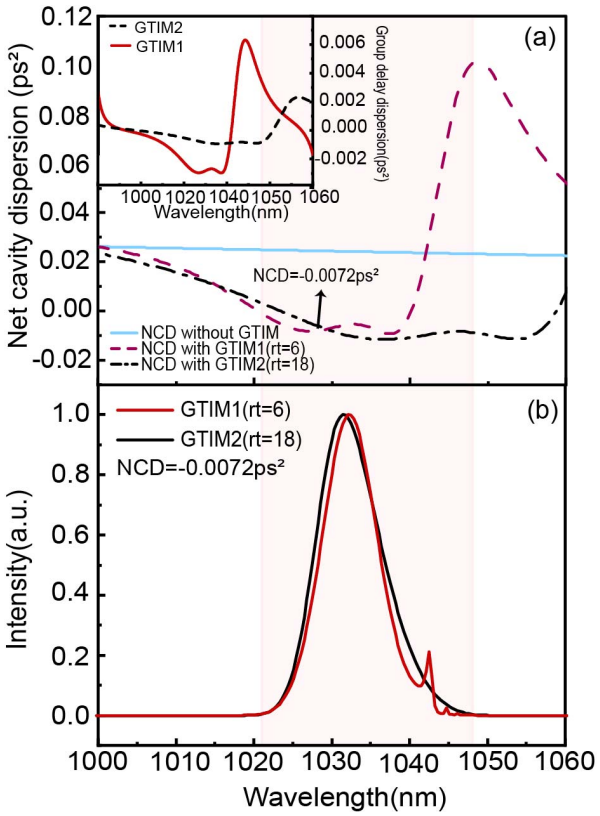

Fig. 2. (a) NCD curve with GTIM1 (reflection for 6 times), GTIM2 (reflection for 18 times), and without the GTI mirrors. The NCD value is −0.0072 ps^2 at 1030 nm after compensation. Inset: the GDD curve of GTIM1 and GTIM2. (b) Spectra when using GTIM1 and GTIM2 for dispersion compensation separately, whose NCD curves correspond to the red line and the black line in (a).

laser, the second-order dispersion to tenth-order dispersion of the GTI mirrors are considered in the simulation.

When we use GTIM2 for dispersion compensation, the spectrum has a Gaussian shape. However, when we use GTIM1, a sideband appears on the right side of the spectrum. In the case of using GTIM1, the pink zone in Fig. 2 shows that the laser pulses experience a rapid change of NCD over this spectral range so that the influence of third-order dispersion (TOD) is significant and cannot be ignored. However, unlike the Kelly sidebands in conventional solitons, which are multiple and symmetrically distributed on both sides, the sideband here is caused by the introduction of HOD, especially the TOD of the GTI mirrors. In such conditions, the phase-matching condition can be written as

$$\Delta\omega_d^2 + \frac{D_3}{3D}\Delta\omega_d^3 = -\left(\frac{1}{T^2}\right), \tag{3}$$

$$\Delta\omega_d \approx -\frac{D_2}{D_3}, \tag{4}$$

where $T = \tau/1.76$, and τ is pulse duration. $\Delta\omega_d = \omega_d - \omega_s$, ω_d, ω_s represent the frequency of the sideband and spectrum center. $\Delta\omega_d$ is positively correlated with the ratio of the NCD to the NTOD. By calculation, the ratio at the center wavelength is approximately equal to 12.5, which is positive, so that the sideband will only appear on the right side. It is seen from the red curve of Fig. 2(b) that the sideband causes the main peak of the spectrum to become narrower than the main peak of the black curve. From the simulation above, we arrive at the conclusion that using various GTI mirrors will induce different HOD and present different spectrum result. Sometimes, in order to compensate for the positive dispersion introduced by long fibers in low repetition rate lasers, we inevitably use mirrors such as GTIM1 to provide sufficient GDD. In such situations, we have to find other ways to resolve the sideband problems.

We will now use the numerical model above to study the following three main parameters of the laser: (1) the transmission coefficient of the output mirror; (2) the gain saturation energy E_{sat}, which corresponds to the pump power in the experiment; and (3) the ratio of the NCD to the NTOD. In particular, we will study the effect of these parameters on the spectral sidebands. From the previous discussion in Section 2, we know that the wavelengths of the sidebands caused by HOD are related to the ratio of the NCD to the NTOD. Consequently, there is a strong possibility that adjusting the reflection times of the GTI mirrors can optimize this ratio indirectly so as to suppress spectral sidebands. To remain consistent with the experiment, we changed the ratio of the NCD to the NTOD by changing the reflection times of the GTI mirrors in the simulation. In order to precisely adjust the NCD value in the near-zero dispersion region and observe its influence on the sidebands, GTIM1 and GTIM2 are used together to compensate for the dispersion. We set the number of reflections in GTIM1 to two and increase the reflections in GTIM2 (Times_2) from ten to twenty in steps of two. The corresponding NCD ranges from $-0.0032\ ps^2$ to $-0.0232\ ps^2$.

In this work, the increasing NCD means that the absolute value of the NCD increases. As the NCD increases, the spectrum becomes narrower while the sideband slightly moves to the longer wavelength region, and its energy gets weaker, as shown in Fig. 3(a). Essentially, the changes in sideband are because the NCD-to-NTOD ratio has changed as the Times_2 increases, as displayed in Fig. 3(b). That is to say, in our laser the wavelength and energy of the sideband can be tuned by changing the reflection times of the GTI mirrors. Consequently, by continually increasing the NCD, we can obtain a spectrum without sidebands, but the NCD should not be too large, otherwise the pulse duration will be longer. Under these circumstances, it is necessary to cooperate with other methods in order to optimize the sideband so as not to increase the pulse duration due to excessive increase of the NCD.

Spectra at different gain saturation energies E_{sat} have been studied in Fig. 3(c). As the E_{sat} increases from 0.05 nJ to 0.3 nJ, the spectrum gets wider, and the sideband becomes stronger. This means that a lower E_{sat} corresponds to a lower sideband, and the sideband will be eliminated by decreasing E_{sat}. According to relevant literature studies[19], the dispersive wave is proportional to the energy of the soliton. Thus, when

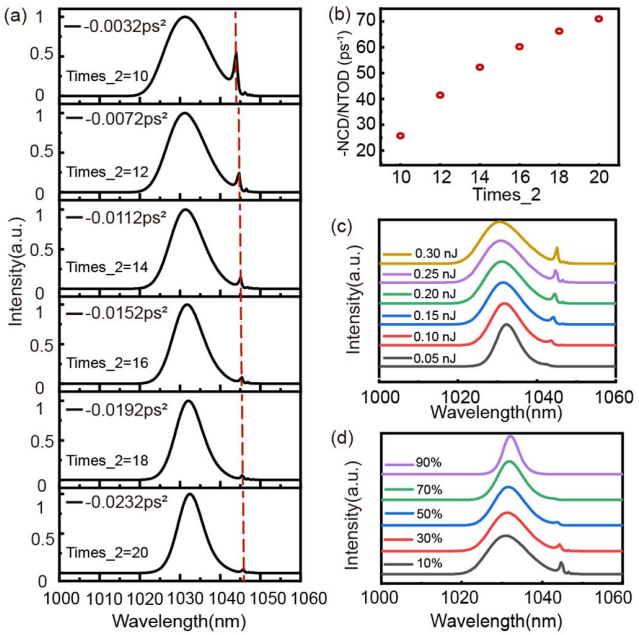

Fig. 3. Simulation results. (a) The spectra at different NCD. Times_2 represents the reflection times of GTIM2. (b) The ratio of the NCD to the NTOD versus Times_2, which corresponds to (a). (c) The spectra at different gain saturation energies E_{sat}. (d) The spectra at different transmission coefficients of the output mirror.

the gain saturation energy becomes stronger, the soliton becomes stronger and so does the dispersion wave. When the phase matching condition is met, the spectral sidebands formed by the interference between soliton and dispersive wave will also be stronger. This means that a lower E_{sat} corresponds to a lower sideband, and the sideband will be eliminated by decreasing E_{sat}. However, the output power will also be reduced if we decrease the E_{sat}. Increasing the transmission coefficient of the output mirror is a way to address this problem. This would suppress the sideband without reducing the output power. Figure 3(d) shows the situation for different transmission coefficients of the output mirror. As the transmission coefficient increases, the spectral sideband begins to lower and the spectral width gets narrower. Different transmission coefficients mean different losses so that lower transmission coefficients correspond to higher soliton energies in the cavity. Increasing the transmission coefficient is another way to adjust the energy in cavity without reducing the output power, compared with decreasing E_{sat}. The above simulation results provide guidance for the experiment.

3. Experimental Setup and Results

According to the numerical simulations above, a linear cavity mode-locked fiber laser with dispersion-compensating GTI mirrors is built, as shown in Fig. 4. The highly Yb-doped fiber (CorActive, PM-Yb401) is 0.28 m long. The pump light emitted by a 976-nm LD pump source is coupled into the gain fiber through a polarization-maintaining wavelength division

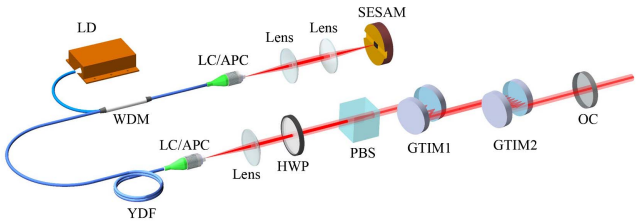

Fig. 4. Configuration of the dispersion-managed mode-locked fiber laser with GTI mirrors. Laser diode, LD; wavelength division multiplexer, WDM; Yb-doped fiber, YDF; single-mode fiber, SMF; semiconductor saturable absorber mirror, SESAM; half-wave plate, HWP; GTIM1, GTI mirrors of −3000 fs^2; and GTIM2, GTI mirrors of −1000 fs^2; output coupler, OC.

multiplexer. The SESAM has a modulation depth of 34% and a recovery time of 700 fs, which acts as an end mirror at one end of the linear cavity. The GTI mirrors require the incident light to be horizontally polarized, so we put a polarization beam splitter (PBS) in front of the GTI mirrors for polarization control. A half-wave plate is placed in front of the PBS to adjust the polarization state of the returned light to align it with the fast and slow axes of the polarization-maintaining fiber. For a single reflection, the GDDs of the GTI mirrors are −3000 fs^2 (Ultrafast Innovation, HD73) and −1000 fs^2 (Layertec, 105195), respectively. The output spectrum is measured with an optical spectrum analyzer (Yokogawa, AQ6370B), and the time-domain intensity is measured by an autocorrelator (APE, Pulse Check).

In the experiment, the pump power is 90 mW. The number of reflections in GTIM1 is fixed at two, and the number of reflections in GTIM2 can be varied from 10 to 20, corresponding to a range of variation in the NCD from −0.0032 ps^2 to −0.0232 ps^2. In fact, we indirectly change the ratio of the NCD to the NTOD when changing the reflections in GTIM2, which is the same as in the simulation. Furthermore, with a change of the reflections in GTIM2, stable mode-locking can be achieved in this wide NCD range. Figure 5(a) presents the spectral results under different NCD values. It is clear from the figure that the energy of the sideband gets increasingly weaker as the NCD increases. At the same time, the central wavelength of the sideband moves toward longer, which is consistent with the simulation. Through simulation and experiment in the near-zero negative dispersion regime, we conclude that increasing the number of reflections in the GTIM2, namely, increasing the ratio of the NCD to the NTOD, can lead to a sideband-free spectrum. Figure 5(b) shows the spectra with the pump power tuned from 70 mW to 130 mW. As the pump power increases, the output spectrum is broadened and the sideband becomes stronger. A lower pump power is helpful for producing a sideband-free spectrum but will lead to a lower output power. This is consistent with the simulation displayed in Fig. 3(c). Notably, the position of the sideband moves toward the longer wavelengths with the pump power, which contradicts the position of the sidebands in conventional solitons. This phenomenon can be explained according to the phase-matching conditions shown in Eq. (3). When

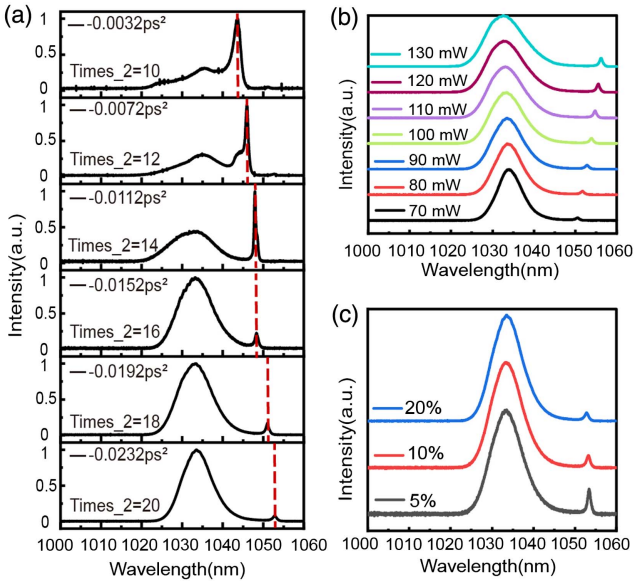

Fig. 5. Experimental results. (a) The spectra at different NCD values. Times_2 represents the reflection times of GTIM2. (b) The spectra under different pump powers. (c) The spectra under different transmission coefficients.

the pump power increases, the spectral width will become wider, and the corresponding pulse duration will become narrower. Then, the $\Delta\omega_d$ will become larger, which means that the position of the sideband will move toward a longer wavelength.

Figure 5(c) demonstrates the spectra under different transmission coefficients of the output mirror in the experiment. Under a pump power of 90 mW, output coupling mirrors with transmission coefficients of 5%, 10%, and 20% are used to explore the influence of the output coupling mirrors on the laser output spectrum. The same behaviors are obtained in both the simulation and the experiment: as the transmission coefficient increases, the sideband energy becomes weaker. In the simulation, the transmission coefficient can be made very large, so the spectral bandwidth is narrowed. In the experiment, due to the limitations on the transmission coefficients, the spectral width does not change significantly, but we can see from Fig. 5(c) that the trend of the spectral sidebands is similar to those in the simulation. The sideband energy can also be controlled by changing the loss in the cavity via adjusting the angle of the output coupling mirror, but like decreasing the pump power, this will reduce the output power. However, in contrast to decreasing the pump power and adjusting the angle of the output coupling mirror, increasing the transmission coefficient will increase the output power. By increasing the transmission coefficient of the output mirror, as shown in Table 1, the spectral width is only reduced by a few tenths of a nanometer. But this method produces a higher output power and a wider mode-locking interval, and helps to suppress sidebands.

According to the simulation and experimental results, optimizing (1) the transmission coefficient of the output mirror, (2) the pump power, and (3) the ratio of the NCD to the NTOD in the cavity can suppress sidebands. The fiber length in our laser is relatively short, so we take GTIM1 away from the laser cavity and only use GTIM2, which has a relatively flat dispersion curve but a small GDD to compensate for dispersion. This greatly reduces the HOD and therefore avoids the dispersive waves caused by the HOD disturbance, and thus reduces the probability of the appearance of spectral sidebands. Moreover, we further optimize these three parameters. When GTIM2 is set to reflect light 26 times, which corresponds to an NCD of -0.0232 ps^2, the pump power is 90 mW and transmission coefficient is 20%, and we can obtain a wide and sideband-free spectrum at near zero dispersion, as shown in Fig. 6.

Table 1. Summary of the Output Laser Parameters under Different Transmission Coefficients of the Output Mirror.

Output Coupling Ratio	Spectral Width (nm)	Pump Power Range of Mode-locking (mW)	Output Power (mW) P_p = 90 mW
5%	8.98	60–170	0.93
10%	8.76	60–185	1.81
20%	8.50	70–200	3.99

As shown in Fig. 6(a), the output spectrum has a full-width at half-maximum of 13.62 nm (the resolution is 0.05 nm), an almost perfect Gaussian shape, and no spectral sidebands are generated. Note that there are two small symmetrical peaks at the bottom of the spectrum in the logarithmic scale with wavelengths of 1021 nm and 1053.5 nm, respectively. However, the experiments prove that the peaks nearly do not change with the pump power and the NCD, so we do not regard them as sidebands. It is possible that the measurement, or other reasons, cause the peaks to appear. Figure 6(b) is the corresponding

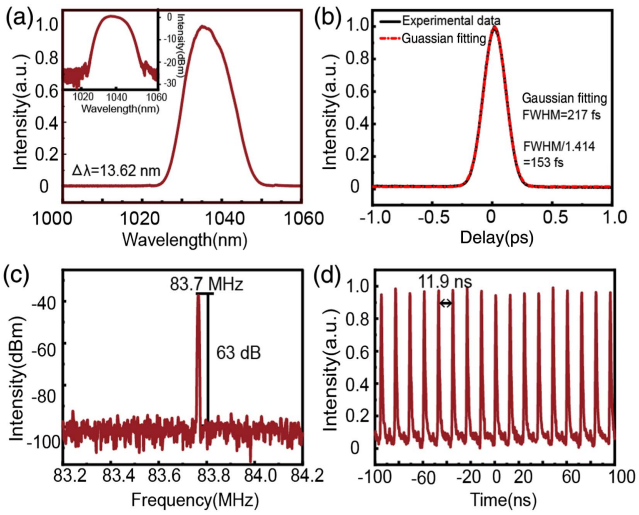

Fig. 6. Mode-locked fiber laser output characteristics at 90 mW pump power. (a) The spectrum in the linear scale (the inset is the spectrum in the logarithmic scale), (b) the intensity autocorrelation trace, (c) the output RF spectrum, and (d) the typical pulse train.

autocorrelation trace, where the pulse duration based on a Gaussian function fitting is 153 fs. The measured RF spectrum is illustrated in Fig. 6(c), and the signal-to-noise ratio is 63 dB at a resolution bandwidth of 3 kHz, indicating that good stability is obtained for the laser mode locking. The output power is 5.14 mW. An oscilloscope pulse sequence is shown in Fig. 6(d), and the corresponding pulse interval is 11.9 ns, which matches the cavity length. The repetition rate of the laser is 83.7 MHz. For longer fibers, we can also use GTI mirrors with a smaller dispersion, which will provide a flat dispersion curve for multiple reflections to compensate for the dispersion so that the HOD will be reduced. Combined with the optimization of the transmission coefficient of the output mirror and the pump power, there is the potential to achieve a wider spectrum without sidebands.

4. Conclusion

In conclusion, we have proposed a pathway for producing a sideband-free spectrum in a dispersion-managed mode-locked fiber laser with GTI mirrors in the near-zero dispersion region. In this region, we have numerically and experimentally investigated the effects of the output spectrum on the transmission coefficient of the output mirror, the ratio of the NCD to the NTOD, and the pump power. The results indicate that optimizing these three parameters can suppress spectral sidebands. As proof of that, only the GTI mirrors with a flat dispersion curve but small GDD are used to reflect light 26 times, so as to reduce the HOD. Then optimizing the three aforementioned parameters, we obtain a nearly perfect Gaussian-shaped spectrum with a spectral width of 13.62 nm, which corresponds to a pulse duration of 153 fs at an NCD of $-0.0232\,\mathrm{ps}^2$. The output power is 5.14 mW under a repetition rate of 83.7 MHz. Our work provides a comprehensive scheme for mode-locked fiber lasers with GTI mirrors for suppressing spectral sidebands in the near-zero dispersion region. In the future, to accommodate fiber lasers with longer fiber and lower repetition rates, a possible promising approach is to choose GTI mirrors with a large size, a small amount of dispersion, and a flat dispersion curve for multiple reflections in order to reduce the HOD. In this case, if the sideband still exists, we can optimize the three parameters mentioned above to eliminate sidebands and output a sideband-free spectrum.

Acknowledgement

This work was partially supported by the National Key Research and Development Program of China (No. 2021YFB3602600) and the Research and Development Program in Key Areas of Guangdong Province, China (No. 2020B090922004).

References

1. I. Hartl, G. Imeshev, L. Dong, G. C. Cho, and M. E. Fermann, "Ultra-compact dispersion compensated femtosecond fiber oscillators and amplifiers," in *Conference on Lasers and Electro-Optics* (Optica Publishing Group, 2005), paper CThG1.
2. F. D. Nielsen, M. Ø. Pedersen, Y. Qian, T. V. Andersen, L. Leick, K. P. Hansen, C. F. Pedersen, and C. L. Thomsen, "High power polarization maintaining supercontinuum source," in *European Conference on Lasers and Electro-Optics and the International Quantum Electronics Conference* (Optica Publishing Group, 2007), paper CJ5_4.
3. I. Hartl, T. R. Schibli, A. Marcinkevicius, D. C. Yost, D. D. Hudson, M. E. Fermann, and J. Ye, "Cavity-enhanced similariton Yb-fiber laser frequency comb: 3×10^{14} W/cm^2 peak intensity at 136 MHz," Opt. Lett. **32**, 2870 (2007).
4. K. C. Phillips, H. H. Gandhi, E. Mazur, and S. K. Sundaram, "Ultrafast laser processing of materials: a review," Adv. Opt. Photonics **7**, 684 (2015).
5. K. Sugioka and Y. Cheng, "Ultrafast lasers–reliable tools for advanced materials processing," Light Sci. Appl. **3**, e149 (2014).
6. M. Malinauskas, A. Žukauskas, S. Hasegawa, Y. Hayasaki, V. Mizeikis, R. Buividas, and S. Juodkazis, "Ultrafast laser processing of materials: from science to industry," Light Sci. Appl. **5**, e16133 (2016).
7. M. E. Fermann and I. Hartl, "Ultrafast fibre lasers technology," Nat. Photonics **7**, 868 (2013).
8. M. Guan, D. Chen, S. Hu, H. Zhao, P. You, and S. Meng, "Theoretical insights into ultrafast dynamics in quantum materials," Ultrafast Science **2022**, 9767251 (2022).
9. X. Li, W. Xu, Y. Wang, X. Zhang, Z. Hui, H. Zhang, S. Wageh, O. A. Al-Hartomy, and A. G. Al-Sehemi, "Optical-intensity modulators with PbTe thermoelectric nanopowders for ultrafast photonics," Appl. Mater. Today **28**, 101546 (2022).
10. X. Li, M. An, G. Li, Y. Han, P. Guo, E. Chen, J. Hu, Z. Song, H. Lu, and J. Lu, "MOF-derived porous dodecahedron rGO-Co_3O_4 for robust pulse generation," Adv. Mater. Interfaces **9**, 2101933 (2022).
11. M. E. Fermann and I. Hartl, "Ultrafast fiber laser technology," IEEE J. Sel. Top. Quantum Electron. **15**, 191 (2009).
12. K. Tamura, E. P. Ippen, H. A. Haus, and L. E. Nelson, "77-fs pulse generation from a stretched-pulse mode-locked all-fiber ring laser," Opt. Lett. **18**, 1080 (1993).
13. C. K. Nielsen, B. Ortaç, T. Schreiber, J. Limpert, R. Hohmuth, W. Richter, and A. Tünnermann, "Self-starting self-similar all-polarization maintaining Yb-doped fiber laser," Opt. Express **13**, 9346 (2005).
14. P. Grelu and N. Akhmediev, "Dissipative solitons for mode-locked lasers," Nat. Photonics **6**, 84 (2012).
15. A. Rosenthal and M. Horowitz, "Analysis and design of nonlinear fiber Bragg gratings and their application for optical compression of reflected pulses," Opt. Lett. **31**, 1334 (2006).
16. J. D. Kafka and T. Baer, "Prism-pair dispersive delay lines in optical pulse compression," Opt. Lett. **12**, 401 (1987).
17. J. Niu, B. Liu, H. Song, S. Zhao, S. Li, T. Wang, X. Gu, L. Chai, and M. Hu, "Femtosecond chirped-pulse amplifier system based on spectrum control and dispersion optimization," Chin. J. Lasers **47**, 0101006 (2020).
18. D. Yan, B. Liu, J. Guo, M. Zhang, Y. Chu, Y. Song, and M. Hu, "Route to stable dispersion-managed mode-locked Yb-doped fiber lasers with near-zero net cavity dispersion," Opt. Express **28**, 29766 (2020).
19. Q. Lin and I. Sorokina, "High-order dispersion effects in solitary mode-locked lasers: side-band generation," Opt. Commun. **153**, 285 (1998).
20. L. A. Gomes, L. Orsila, T. Jouhti, and O. G. Okhotnikov, "Picosecond SESAM-based ytterbium mode-locked fiber lasers," IEEE J. of Sel. Top. Quantum Electron. **10**, 129 (2004).
21. L. Ren, L. Chen, M. Zhang, C. Zhou, Y. Cai, and Z. Zhang, "Group delay dispersion compensation in an ytterbium-doped fiber laser using intracavity Gires–Tournois interferometers," Opt. Laser Technol. **42**, 1077 (2010).
22. X. Jia, Y. Song, L. Yan, Q. Lin, L. Hou, X. Feng, and J. Bai, "Yb-doped polarization-maintaining femtosecond fiber laser using Gires–Tournois interferometers for dispersion management," Appl. Phys. Express **14**, 112007 (2021).
23. Y. Li, M. Jiang, L. Hou, Y. Song, X. Jia, Z. Ren, and J. Bai, "90-fs Yb-doped fiber laser using Gires–Tournois interferometers as dispersion compensation," Opt. Commun. **529**, 129074 (2023).
24. P. F. Curley, Ch. Spielmann, T. Brabec, F. Krausz, E. Wintner, and A. J. Schmidt, "Operation of a femtosecond Ti:sapphire solitary laser in the vicinity of zero group-delay dispersion," Opt. Lett. **18**, 54 (1993).

25. T. Brabec, S. Kelly, and F. Krausz, "Passive modelocking in solid state lasers," in *Compact Sources of Ultrashort Pulses*, I. N. Durling, III, ed. (Cambridge, 1995), p. 57.
26. K. Smith and L. F. Mollenauer, "Experimental-observation of soliton interaction over long fiber paths-discovery of a long-range interaction," Opt. Lett. **14**, 1284 (1989).
27. S. M. J. Kelly, "Characteristic sideband instability of periodically amplified average soliton," Electron. Lett. **28**, 806 (1992).
28. C. W. Rudy, K. E. Urbanek, M. J. F. Digonnet, and R. L. Byer, "Amplified 2-μm thulium-doped all-fiber mode-locked figure-eight laser," J. Light. Technol. **31**, 1809 (2013).
29. Y. Zhao, L. Yongzhi, Z. Deshuang, L. Huang, and Z. Dai, "Study on side bands in passively mode-locked fiber laser," Acta Opt. Sin. **29**, 991 (2009).
30. J. Li, Y. Wang, H. Luo, Y. Liu, Z. Yan, Z. Sun, and L. Zhang, "Kelly sideband suppression and wavelength tuning of a conventional soliton in a Tm-doped hybrid mode-locked fiber laser with an all-fiber Lyot filter," Photonics Res. **7**, 103 (2019).
31. Y. Wang, S. Fu, J. Kong, A. Komarov, M. Klimczak, R. Buczyński, X. Tang, M. Tang, Y. Qin, and L. Zhao, "Nonlinear Fourier transform enabled eigenvalue spectrum investigation for fiber laser radiation," Photonics Res. **9**, 1531 (2021).
32. Y. Wang, S. Fu, C. Zhang, X. Tang, J. Kong, J. H. Lee, and L. Zhao, "Soliton distillation of pulses from a fiber laser," J. Light. Technol. **39**, 2542 (2021).